Remote Sensing of Environment 253 (2021) 112175

Contents lists available at ScienceDirect

Remote Sensing of Environment

journal homepage: www.elsevier.com/locate/rse

Satellite image texture captures vegetation heterogeneity and explains patterns of bird richness

Laura S. Farwell [a,*], David Gudex-Cross [a], Ilianna E. Anise [b], Michael J. Bosch [b], Ashley M. Olah [a], Volker C. Radeloff [a], Elena Razenkova [a], Natalia Rogova [a], Eduarda M.O. Silveira [a], Matthew M. Smith [a], Anna M. Pidgeon [a]

[a] Department of Forest and Wildlife Ecology, University of Wisconsin-Madison, 1630 Linden Drive, Madison, WI 53706, USA
[b] Department of Integrative Biology, University of Wisconsin-Madison, 250 North Mills Street, Madison, WI 53706, USA

ARTICLE INFO

Keywords:
Biodiversity
Enhanced vegetation index (EVI)
Landsat 8
Lidar
National Ecological Observatory Network (NEON)
Sentinel-2
Vegetation composition
Vegetation structure

ABSTRACT

Addressing global declines in biodiversity requires accurate assessments of key environmental attributes determining patterns of species diversity. Spatial heterogeneity of vegetation strongly affects species diversity patterns, and measures of vegetation structure derived from lidar and satellite image texture analysis correlate well with species richness. Our goal here was to gain a better understanding of why image texture explains bird richness, by linking field-based measures of vegetation structure directly with both image texture and bird richness. In addition, we asked how image texture compares with lidar-based canopy height variability, and how sensor resolution affects the explanatory power of image texture. We generated texture metrics from 30 m (Landsat 8) and 10 m (Sentinel-2) resolution Enhanced Vegetation Index (EVI) imagery from 2017 to 2019. We compared textures with vegetation metrics and bird richness data from 27 National Ecological Observatory Network (NEON) terrestrial field sites across the continental US. Both 30 and 10 m resolution texture metrics were strongly correlated with lidar-based canopy height variability ($|r| = 0.64$ and 0.80, respectively). Texture was moderately correlated with field-based metrics, including variability of vegetation height and tree stem diameter, and foliage height diversity (range $|r| = 0.31$–0.52). Generally, 10 m resolution texture had stronger correlations with lidar and field-based metrics than 30 m resolution texture. In univariate linear models of total bird richness, 10 m resolution texture metrics also had higher explanatory power (up to $R^2_{adj} = 0.45$), than 30 m texture metrics (up to $R^2_{adj} = 0.31$). Among all metrics evaluated, the 10 m homogeneity texture was the best univariate predictor of total bird richness. In multivariate bird richness models that combined texture with lidar-based canopy height variability and field-based metrics, both 30 m and 10 m resolution texture metrics were selected in top-ranked models and independently contributed explanatory power (up to $R^2_{adj} = 46\%$). Lidar-based canopy height variability was also selected in a top-ranked model of total bird richness, but independently contributed only 15% of the variance explained. Our results show satellite image texture characterized multiple features of structural and compositional vegetation heterogeneity, complemented more commonly used metrics in models of bird richness and for some guilds outperformed both lidar-based canopy height variability and field-based vegetation measurements. Ours is the first study to directly link image texture both to specific components of vegetation heterogeneity and to bird richness across multiple ecoregions and spatial resolutions, thereby shedding light on habitat features underlying the strong correlation between image texture and biodiversity.

1. Introduction

The Earth's ecosystems are undergoing rapid changes and unprecedented declines in biological diversity (Cardinale et al., 2012). There is a pressing need for accessible and reliable measures of key environmental determinants of biodiversity to help guide and monitor conservation strategies (Pettorelli et al., 2016; Jetz et al., 2019). Environmental heterogeneity is a powerful predictor of biodiversity patterns (Stein et al.,

* Corresponding author.
E-mail address: lfarwell@wisc.edu (L.S. Farwell).

https://doi.org/10.1016/j.rse.2020.112175
Received 2 July 2020; Received in revised form 9 October 2020; Accepted 3 November 2020
Available online 12 November 2020

2014), and spatial heterogeneity of vegetation has a particularly strong influence on species distributions and diversity (MacArthur and MacArthur, 1961; Tews et al., 2004). Vegetation heterogeneity affects biodiversity patterns by influencing resource use and selection (Cody, 1968; Patthey et al., 2012), species interactions (Loarie et al., 2013; Seibold et al., 2013) and movement patterns (Frair et al., 2005; Jirinec et al., 2016). Spatial heterogeneity of vegetation can also increase microenvironmental conditions that serve as refugia from climatic extremes (Virah-Sawmy et al., 2009; Melin et al., 2014).

Both the structural and the compositional heterogeneity of vegetation increase species diversity at a range of spatial scales by increasing the variety of available resources and diversity of ways animals can exploit those resources (Benton et al., 2003; Schuldt et al., 2019). Vegetation structure refers to the three-dimensional configuration of plants, such as plant height, density, and distribution of vertical layers, while vegetation composition describes the identity and variety of plant species or major lifeforms (Noss, 1990). The structure of vegetation, its physical complexity and arrangement, are important drivers of species diversity (MacArthur and MacArthur, 1961; McCoy and Bell, 1991). However, the floristic composition and diversity of plants also influences animal distributions and interactions (Zhao et al., 2006; Castagneyrol and Jactel, 2012). Vegetation heterogeneity thus plays a complex and important role in determining patterns of biodiversity.

Vegetation heterogeneity is difficult to quantify and measuring it across broad areas is a challenge which entails trade-offs among different methods. Field-based methods quantify plant structural and compositional heterogeneity directly but have limited coverage in time and space (Rocchini et al., 2010). Lidar imaging is a fine-resolution alternative for estimating vegetation structure but is costly to obtain, has limited spatial and temporal coverage (Simonson et al., 2014), often excludes lower vegetation layers, and provides little information on composition. Satellite-based remote sensing data typically only measure proxies of structural and compositional heterogeneity, but provide continuous measures for large areas (Rocchini et al., 2016) and can quantify and map vegetation characteristics that are important for biodiversity (Pettorelli et al., 2016; Wang and Gamon, 2019). These different types of vegetation data thus have different strengths and drawbacks and are most powerful and informative when used in combination (Rhodes et al., 2015; Rocchini et al., 2016).

Satellite image texture analysis is an approach that shows particular promise for characterizing aspects of habitat structure and composition over broad extents (Bellis et al., 2008; Farwell et al., 2020). Image texture quantifies spectral and spatial variations in pixel values of an image, and thus conveys information about the spectral and spatial heterogeneity of image features (Haralick et al., 1973). Texture metrics based on productivity measures, including the normalized difference and enhanced vegetation indices (NDVI, EVI), provide important information about spatial patterns in vegetation structure and composition (St-Louis et al., 2009; Campos et al., 2018). Indeed, texture analyses of satellite images at varying resolutions have been used to effectively characterize patterns of both structural and compositional vegetation heterogeneity across a range of habitat types, such as successional stages in coniferous forests (30 m; Jakubauskas, 1997), stand structure metrics in coniferous plantations (1–3 m; Kayitakire et al., 2006; Ozdemir and Karnieli, 2011), foliage height diversity in a grassland-savanna-woodland mosaic (30 m; Wood et al., 2012), and heterogeneity in plant species composition and structure in dry woodlands (30 m; Campos et al., 2018) and grasslands (15–20 m; Briggs and Nellis, 1991; Guo et al., 2004).

Satellite image texture is also a powerful predictor of biodiversity within different habitats, including forests (Culbert et al., 2012; Wallis et al., 2016), grasslands (Bellis et al., 2008; Culbert et al., 2012), arid shrublands (St-Louis et al., 2009), and savanna-woodland mosaics (Wood et al., 2013). Additionally, EVI-based textures based on Landsat (30 m; Farwell et al., 2020) and MODIS (250 m; Tuanmu and Jetz, 2015) effectively model broad-scale bird richness patterns across the conterminous US. Despite strong correlations between image texture and species richness, however, the underlying habitat features determining these relationships remain unclear (St-Louis et al., 2009; Farwell et al., 2020). While image texture has been linked with particular features of vegetation heterogeneity (e.g., Ozdemir and Karnieli, 2011; Wood et al., 2012), *or* with patterns of bird richness (see above), no prior study has connected texture directly with both vegetation characteristics and bird richness data across multiple habitat types and ecoregions. Furthermore, there is a need to identify the spatial resolution of image texture that best characterizes patterns of vegetation heterogeneity relevant for biodiversity (Bar-Massada et al., 2012).

Here, our primary goal was to address these knowledge gaps by (1) identifying which features of vegetation heterogeneity are best captured by image texture across a variety of habitats, ecoregions, and spatial resolutions, and (2) comparing the performance of texture with lidar-based canopy height variability and field-based vegetation metrics in models of bird richness.

- Our first objective was to calculate a suite of image texture metrics based on 30 m (Landsat 8) and 10 m (Sentinel-2) resolution EVI imagery, as well as vegetation metrics from lidar canopy height models and field-based sampling.
- Second, we evaluated correlations between satellite-based texture metrics and more commonly used lidar- and field-based measures of vegetation heterogeneity. We predicted that image texture would have a positive relationship with both vegetation structural and compositional heterogeneity.
- Third, we compared the performance of texture, lidar-based canopy height variability, and field-based measures of vegetation heterogeneity in models of bird richness. We predicted that satellite-based texture would have higher explanatory power than field-based metrics but comparable explanatory power to lidar-based canopy height variability, because image texture and lidar provide continuous habitat measures while field-based metrics have limited spatial coverage.
- Finally, we evaluated the relative importance of image texture in multivariate models of bird richness that also included lidar-based canopy height variability and field-based metrics. We predicted that image texture would complement more common metrics of vegetation heterogeneity and contribute independent explanatory power in models of bird richness.

2. Methods

2.1. Study area

As our study area, we selected 27 of the 44 terrestrial field sites in the National Ecological Observatory Network (NEON) distributed across 16 ecoclimatic domains in the continental US (Barnett et al., 2019a; Fig. 1a; Table S1). NEON partitioned the continent into these domains using multivariate geographical clustering analysis of nine ecoclimatic variables that influence large-scale patterns of vegetation (Thorpe et al., 2016). NEON sites represent the dominant vegetation type within each ecoclimatic domain (Barnett et al., 2019a). We selected sites dominated by forest, grassland, and shrubland habitats (Fig. 2) because these represent broad-scale vegetation associations for breeding birds in the US. Given our main objectives, we only considered sites that provided bird, vegetation, and lidar datasets for the same locations. We used NEON bird sampling plots (750 × 750 m) as our primary unit of analysis, and thus excluded sites too small ($n = 12$) to accommodate full plots (Thorpe et al., 2016). Among the 27 remaining terrestrial sites, we evaluated a total of 223 sampling plots dominated either by forest ($n = 110$), grassland ($n = 53$) or shrubland cover ($n = 52$).

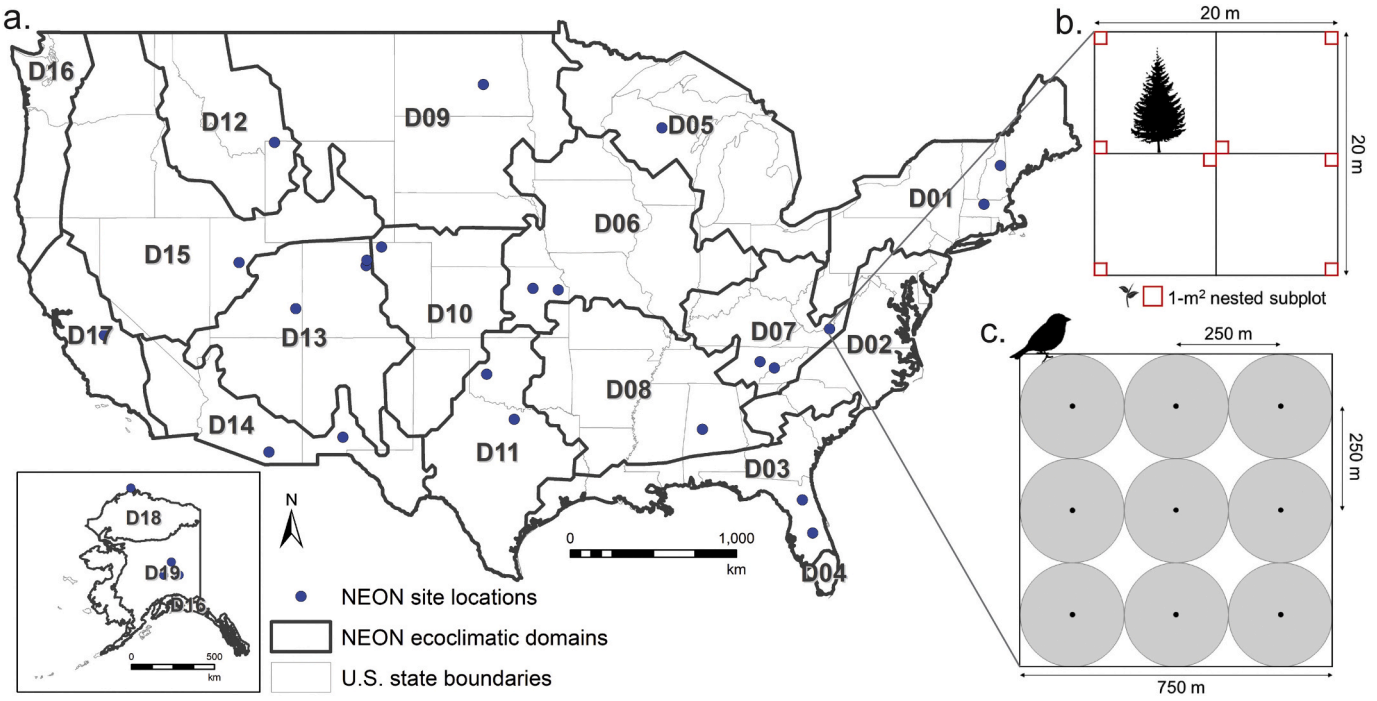

Fig. 1. NEON ecoclimatic domains and terrestrial site locations (a; see Table S1 for full list of domains and sites), with insets showing sampling schematics for vegetation surveys (b) and breeding landbird surveys (c).

2.2. Remote sensing data

2.2.1. Satellite image texture

We calculated image texture metrics from an Enhanced Vegetation Index (EVI) composite for the continental US, derived from Landsat 8 Operational Land Imager atmospherically corrected Surface Reflectance Tier 1 data, and Sentinel-2 Multispectral Instrument Level 2A Bottom of Atmosphere reflectance data. We accessed and processed all satellite images in Google Earth Engine (GEE; Gorelick et al., 2017). We excluded pixels containing water, clouds, or cloud shadows using product quality assessment bands, and those mapped as permanent water bodies based on Landsat imagery (Hansen et al., 2013). We calculated EVI from the near-infrared, red, and blue bands of each image, and chose EVI rather than NDVI because it is less likely to saturate over high biomass and less sensitive to atmospheric conditions and soil brightness (Huete et al., 2002). We used imagery from 2017 to 2019 to match the available NEON bird data, and calculated the median EVI value for each pixel from all available images between March–August as a measure of vegetation greenness during the growing season (Creech et al., 2016). Because negative values were rare in our median EVI composite and generally indicated a lack of vegetation (e.g., rock, bare ground), we set negative values to zero and linearly rescaled EVI values to unsigned 8-bit integers ranging from 1 to 100 for the entire continental US prior to summarizing data for each NEON sampling plot.

In image texture analysis, a texture value is calculated from the spectral values (or 'gray-levels') of all the pixels within a given unit of analysis (Hall-Beyer, 2017). First-order texture metrics are statistical summaries (e.g., mean, variance) of pixel gray-levels within that processing extent, while second-order texture metrics are derived from the gray-level co-occurrence matrix (Haralick et al., 1973). The co-occurrence matrix contains the normalized frequencies with which adjacent pixel gray-levels co-occur within the unit of analysis, and thus reflect spatial patterns and relationships among neighboring pixels (Hall-Beyer, 2017). We calculated first-order standard deviation and 13 second-order texture metrics, using the *glcmTexture* function in GEE (Haralick et al., 1973, Conners et al., 1984; see Table 1 for list of 14 textures calculated). Our unit of analysis was each NEON bird survey plot (Fig. 1c); plot-level texture metrics were calculated using all the pixels within each 750 × 750 m (56.25 ha) plot, i.e., 25 × 25 Landsat 8 (30 m) pixels, or 75 × 75 Sentinel-2 (10 m) pixels. We analyzed texture only at this extent because texture metrics calculated across varying spatial extents are typically highly correlated and show consistent relationships with patterns of species diversity (St-Louis et al., 2006; Wood et al., 2013). We calculated pairwise Spearman's correlation coefficients among texture metrics to check for collinearity because some texture metrics are known to be highly correlated (Baraldi and Parmiggiani, 1995).

Texture metrics provide information about within-class habitat heterogeneity that categorical land cover classifications cannot capture and contribute additional explanatory power when combined with land cover metrics in models of bird richness (Culbert et al., 2012; Tuanmu and Jetz, 2015; Farwell et al., 2020). However, we did not include remotely sensed, classified land cover metrics in our analyses because NEON sites are intentionally located in large areas of contiguous land cover (e.g., entire sites where sampling plots are forested, or in grasslands), and thus are ill-suited for analyses of landscape pattern measures such as patch metrics or categorical land cover diversity.

2.2.2. Lidar canopy height model

We analyzed lidar-derived canopy height models (CHM) from NEON's ecosystem structure dataset to characterize vertical canopy structure and heterogeneity (National Ecological Observatory Network, 2020). NEON produces CHMs at a 1 m spatial resolution, with a minimum height of 2 m (Fig. 2c; see NEON.DOC.002837vA for technical details of lidar-derived CHMs). We used lidar data from the year corresponding with the most recent field-based vegetation data (2017–2019). We used zonal statistics in ArcGIS v. 10.5.1 (Environmental Research Systems Institute, 2016) to calculate three relatively straightforward metrics to derive from existing canopy height models: the mean, maximum, and standard deviation (SD) of canopy height. We calculated these CHM metrics within each 750 × 750 m (56.25 ha) NEON bird sampling plot, also matching the sampling extent of satellite image textures. Because all three CHM metrics were highly correlated ($|r| = 0.91–0.92$), we only included SD of canopy height as a

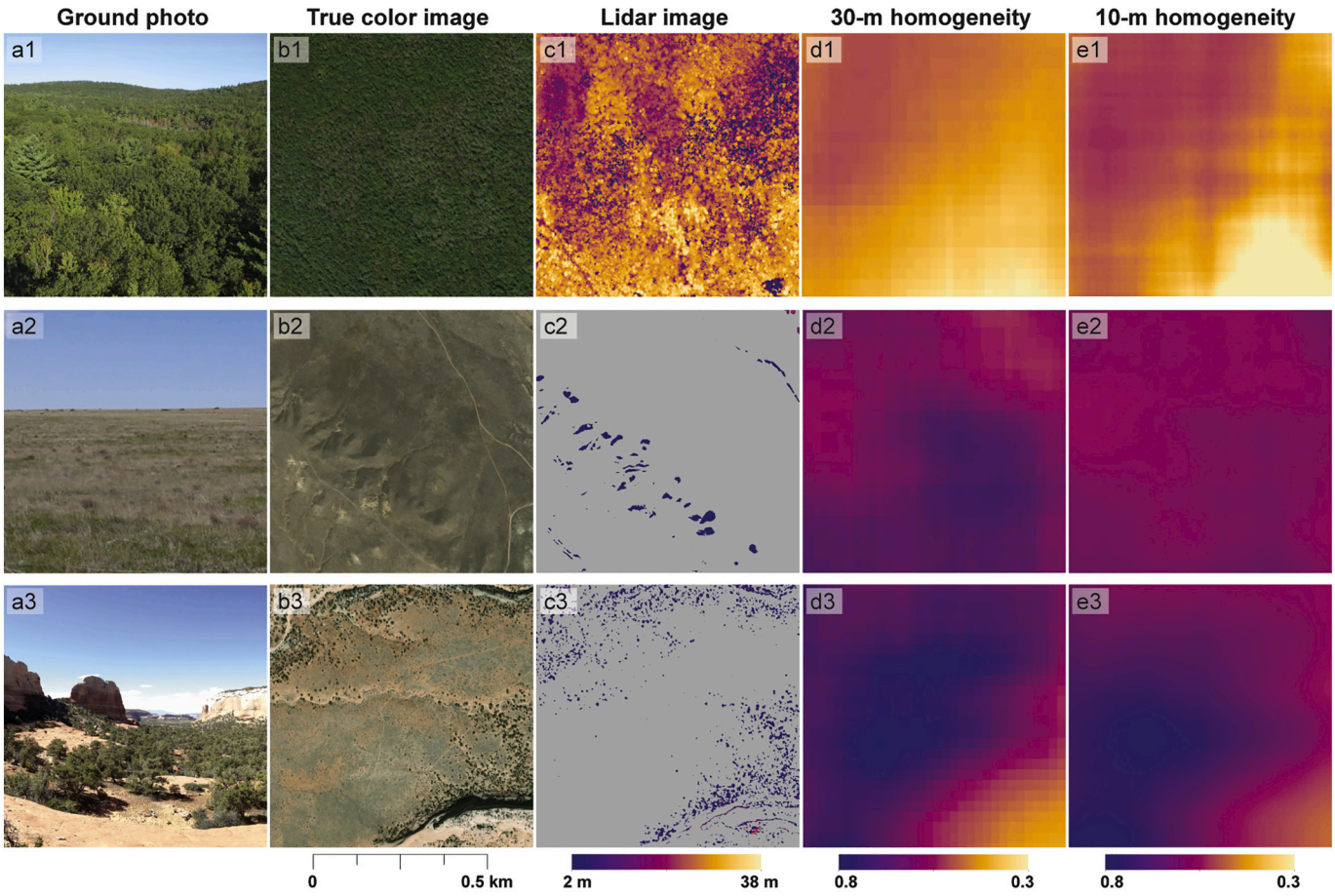

Fig. 2. Data layers (columns a–e) corresponding to three sampled landscapes (rows 1–3), representing forest, grassland, and shrubland habitats: (1) mixed evergreen-deciduous forest in the northeastern US (42°25′47″ N, 72°14′23″ W); (2) shortgrass prairie in the Central Plains of Colorado (40°51′8″ N, 104°44′35″ W); and (3) shrubland in the Moab Desert, in southwestern US (38°15′19″ N, 109°22′31″ W). Columns: (a) ground photo; (b) true color satellite image (Maxar <0.5 m imagery); (c) lidar-derived canopy height model; (d) 30 m homogeneity texture (Landsat 8); and (e) 10 m resolution homogeneity texture (Sentinel-2). Low homogeneity values (yellow) indicate high spatial heterogeneity of vegetation, while high homogeneity values (purple) indicate low heterogeneity. Squares represent 750 × 750 m field sampling plots. (For interpretation of the references to color in this figure legend, the reader is referred to the web version of this article.)

representative measure of lidar-based canopy height variability, in subsequent analyses. The minimum height of 2 m for CHMs resulted in limited variability of canopy height data in grasslands, and to a lesser extent in shrublands. Thus, analyses of metrics derived from lidar canopy height in these habitats should be interpreted with caution.

2.2.3. *Field-based vegetation metrics*

To derive field-based vegetation metrics, we analyzed NEON woody plant vegetation structure (WPVS) and plant presence and percent cover (PPPC) datasets (National Ecological Observatory Network, 2020). WPVS data (e.g., height, stem diameter) are collected for all trees and shrubs within 20 × 20 m plots, which are distributed across each site using a stratified random approach (Thorpe et al., 2016; Fig. 1b). PPPC data are collected in 6–8 smaller plots (1 m^2) nested within the larger WPVS plots (Barnett et al., 2019b; Fig. 1b). We only included vegetation plots co-located with bird sampling plots in our analyses ($n = 223$); sites contained a range of 1–13 co-located sampling plots (mean = 8.3). NEON uses standardized vegetation sampling protocols across all terrestrial sites. However, WPVS data is only collected if at least one tree with a stem diameter ≥ 10 cm is present, or if woody plants constitute ≥10% cover of the plot. Thus, WPVS data are not available for all sampling plots, and resulted in limited vegetation structure data for habitats dominated by grass and herbaceous vegetation.

We derived a suite of field-based vegetation metrics from WPVS and PPPC data. We calculated SD of woody vegetation height for each plot, as a field-based measure of variability in vertical vegetation structure. We categorized height data for shrubs and trees into four height bins representing different woody vegetation layers (Lopatin et al., 2015): low canopy (0–2 m), middle-low canopy (2–8 m), middle-high canopy (8–16 m), and high canopy (> 16 m). To characterize foliage height diversity, or the distribution of woody vegetation among these vertical layers, we calculated the Shannon diversity index (SDI) because it accounts for both the abundance and evenness of vegetation layers, and is a commonly used and standard metric for quantifying environmental variability (e.g., MacArthur and MacArthur, 1961; Ozdemir et al., 2018). For trees with a stem diameter > 10 cm, we calculated basal area and SD of tree stem diameter as measures of tree volume/density and variability in tree size, respectively. Based on the North American plant species dataset developed by Engemann et al. (2016), we classified plant species into six lifeforms, and converted PPPC data for individual species to percent cover for each major lifeform: herbaceous broadleaf plants, grasses, vines, non-woody epiphytes, shrubs, and trees. In subsequent analyses, we focus on percent cover of herbaceous broadleaf plants, grasses, shrubs and trees as major plant lifeforms important for birds within our three habitat guilds (forest, grassland, shrubland). Using these major lifeform percent cover values, we also calculated SDI of plant cover types, as a measure of vegetation compositional heterogeneity.

Table 1
Image texture measures selected for analysis, with formulae (Haralick et al., 1973; Conners et al., 1984).

Texture metric	Description	Formula[a]
First order: Standard deviation	Dispersion of pixel values.	$\sqrt{\frac{\sum \lvert x-\overline{x}\rvert^2}{N}}$
Second order: Contrast (also "Sum of squares variance", or "Inertia")	Exponentially weighted difference in adjacent pixels. High values indicate local regions of high contrast.	$\sum_{i,j=0}^{N-1} p(i,j)\ (i-j)^2$
Dissimilarity	Linear difference in values of adjacent pixels.	$\sum_{i,j=0}^{N-1} p(i,j)\ \lvert i-j\rvert$
Homogeneity (also "Inverse difference moment")	Similarity of values between adjacent pixels; smoothness of an image. Low values indicate greater heterogeneity.	$\sum_{i,j=0}^{N-1} \frac{p(i,j)}{1+(i-j)^2}$
Uniformity (also "Angular second moment", or "Energy")	Orderliness in spatial distribution of pixel values.	$\sum_{i,j=0}^{N-1} (p(i,j))^2$
Entropy	Disorderliness (or 'randomness') in spatial distribution of pixel values.	$-\sum_{i,j=0}^{N-1} p(i,j)\ log\ (p(i,j))$
Sum entropy	Disorder related to the gray-level sum distribution of an image.	$-\sum_{i=2}^{2N} p_{x+y}(i) log\left\{p_{x+y}(i)\right\}$
Difference entropy	Disorder related to the gray-level difference distribution of the image.	$-\sum_{i=0}^{N-1} p_{x-y}(i) log\left\{p_{x-y}(i)\right\}$
Difference variance	Places higher weights on adjacent pixels with differing intensity levels that deviate more from the mean.	variance of p_{x-y}
Correlation	Linear dependency of neighboring pixel values (0 = uncorrelated, |1| = perfectly correlated).	$\frac{\sum_{i,j=0}^{N-1}(ij)p(i,j)-\mu_x\mu_y}{\sigma_x\sigma_y}$
Information measure of correlation 1[b]	Information gain (reduction in uncertainty) based on nonlinear dependency of neighboring pixel values.	$\frac{HXY-HXY1}{max\{HX,HY\}}$
Information measure of correlation 2[b]	Correlation coefficient related to mutual information of neighboring pixel values.	$\sqrt{1-exp[-2.0(HXY2-HXY)]}$
Cluster shade	Skewness of the GLCM. High values indicate asymmetry.	$\sum_{i,j=0}^{N-1} p(i,j)\ (i+j-\mu_x-\mu_y)^3$
Cluster prominence	Also a measure of asymmetry. Low values indicate GLCM distribution peaks around the mean.	$\sum_{i,j=0}^{N-1} p(i,j)\ (i+j-\mu_x-\mu_y)^4$

[a] Where N is the number of image gray levels; i indicates the gray-level co-occurrence matrix (GLCM) row, and j is the column; $p(i, j)$ is the $(i, j)^{th}$ entry in the normalized GLCM, or the probability that two gray levels i and j will be adjacent; $p_x(i)$ is the i^{th} entry in the marginal-probability matrix; $p_y(j) = \sum_{i=1}^{N} p(i,j)$; μ_x, μ_y, and σ_x, σ_y, are the means and standard deviations of GLCM row and column sums, respectively.

[b] $HXY = -\sum_{i,j=0}^{N-1} p(i,j)\ log(p(i,j))$ where HX, HY are entropies of p_x, p_y; $HXY1 = -\sum_{i,j=0}^{N-1} p(i,j) log\left\{p_x(i)p_y(j)\right\}$; $HXY2 = -\sum_{i,j=0}^{N-1} p_x(i)p_y(j)\ log\left\{p_x(i)p_y(j)\right\}$.

2.3. Landbird data

We analyzed the NEON breeding landbird point count dataset (National Ecological Observatory Network, 2020) to calculate bird species richness. We limited our bird richness analyses to data collected during 2017–2019, because many NEON terrestrial sites did not have bird survey data prior to 2017. Of the 27 terrestrial sites included in our analyses, 25 had three years and 2 had two years of bird survey data. Sampling methods vary between large and small sites within the NEON network. Larger sites use bird survey plots containing 9-point sampling grids (Fig. 1c; hereafter, 'bird plots'), randomly distributed across sites proportionally to the percent cover of National Land Cover Database classes (NLCD; Homer et al., 2020) with the restriction that >50% of sampling points must fall within one dominant NLCD class (Barnett et al., 2019a). Conversely, smaller sites use single, randomly distributed sampling points. Again, we excluded sites too small to contain the larger sampling grids ($n = 12$) to minimize discrepancies in bird richness resulting from sampling differences.

Following the NEON bird sampling protocol, trained observers wait 2 min after arriving at each point, and then conduct a 6-min count during which every bird seen or heard is recorded (Hanni et al., 2016). Each point is surveyed once per year within a 2–3 week sampling period during peak breeding season dates informed by local experts, during site-specific times of day when birds are most likely to sing and when weather conditions are favorable (Ralph et al., 1993; Hanni et al., 2016). We excluded far-ranging species (e.g., raptors), and species poorly sampled by diurnal point count surveys (e.g., nocturnal species). We also excluded observations >125 m from the observer, to minimize counting individual birds at more than one point (sampling points within NEON bird plots are spaced 250 m apart; Ralph et al., 1993). To calculate plot-level bird richness, we counted the cumulative number of species recorded across all nine sampling points for each plot, and across years (2017–2019) to limit effects of interannual differences in timing and survey conditions. We evaluated data from 223 sampling plots with a total of 58,803 observations of 329 species (Table S2). In addition to calculating total species richness, we calculated richness of specialists within three major habitat types: forest, grassland, and shrubland (Table S2). Specialists are birds strongly affiliated with a single breeding habitat type (International Union for Conservation of Nature and Natural Resources, 2020; Billerman et al., 2020), and of the 329 species evaluated, included 75 forest, 14 grassland, and 27 shrubland specialists.

2.4. Statistical analysis

We first applied correlation analysis to identify basic relationships among our different vegetation metrics. Second, we explored their relationships with bird richness in univariate models. Third, based on these preliminary analyses, we selected a set of representative predictors to test in multivariate models of bird richness and evaluated their relative importance.

To investigate which features of vegetation heterogeneity are well-captured by image texture, first we evaluated the relationship between 30 and 10 m texture metrics, lidar canopy height variability, and field-based metrics using Spearman's correlation coefficients. We then tested each set of environmental variables in univariate models of bird richness after centering and standardizing predictors. We parameterized linear regression models to relate environmental predictors to richness of all species and of forest and grassland specialists, because our data were normally distributed (results not shown). The exception was shrubland specialist richness which conformed more closely to a Poisson distribution, but we found that top-ranked predictors in Poisson generalized linear model outputs for this bird group were consistent with those of linear models (Table S3). Thus, to allow for comparisons across bird groups we applied linear regressions for all bird groups evaluated. In our analyses of habitat specialists, we restricted our analyses to sampled plots dominated by the preferred habitat type (i.e., forest, grassland, shrubland) to focus on vegetation metrics that are important for each habitat group, and determined land cover dominance based on percent cover of NLCD classes.

Lastly, we fitted multivariate models of bird richness that included

six predictors with highest explanatory power from each category of variables evaluated in univariate models (see Results, Section 3.3). Our objective for the multivariate models was not to develop models with the highest possible predictive power, but rather to compare the relative performance of texture metrics with a set of representative, more commonly used metrics of vegetation heterogeneity. We generated linear models with all possible subsets of six predictors and an intercept, and fitted models with 30 and 10 m resolution texture metrics, separately. This resulted in a total of 128 models for each group of birds evaluated: all species, forest specialists, grassland specialists, and shrubland specialists (512 models total). We selected top models based on the Bayesian Information Criterion (BIC), which penalizes over-parameterized models to avoid overfitting (Brewer et al., 2016) but can sometimes result in oversimplified models (Burnham and Anderson, 2004). We checked for correlations among predictors before running multivariate models (Figs. S2, S3), and calculated variance inflation factors (VIFs) for each predictor in top-ranked models as a secondary check for multicollinearity, using a threshold of VIF > 4 to remove variables due to multicollinearity (Booth et al., 1994). Model selection approaches can only measure the relative quality of models, thus we also calculated adjusted coefficients of determination (R^2_{adj}) to determine how much of the variance in bird richness was explained by top-ranking models (Guthery et al., 2005). We assessed the relative influence of predictors on bird richness by comparing standardized regression coefficients as measures of effect size, and conducted hierarchical partitioning analysis on top-ranked models, to calculate the independent and joint contribution of each predictor towards total explained variance (Chevan and Sutherland, 1991). The independent contribution of each predictor represents variance that is uniquely explained by that predictor, whereas joint contributions cannot be distinguished from other predictors due to multicollinearity (Mac Nally, 2000).

To check for spatial autocorrelation of NEON sampling locations, we fitted non-parametric covariance functions and analyzed model residuals in spline correlograms with bootstrap confidence envelopes, using 1000 permutations and a 95% confidence level as our threshold (Bjornstad and Falck, 2001). Data exploration and statistical analyses were conducted in R version 3.6.1 (R Core Team, 2020). We used the package "MuMIn" for multivariate models and BIC model selection (Barton, 2019), "car" to calculate VIFs (Fox and Weisberg, 2019), "hier.part" for hierarchical partitioning analysis (Walsh and Mac Nally, 2013), and "ncf" for spline correlograms (Bjornstad, 2020; see Table S4 for descriptions of R packages and functions used).

3. Results

3.1. Vegetation heterogeneity captured by texture

We found positive relationships between texture metrics calculated from EVI composites and multiple lidar- and field-based measures of vegetation structural and compositional heterogeneity (Table 2). Both 30 m (Landsat 8) and 10 m (Sentinel-2) texture metrics showed the strongest relationships with lidar-based canopy height variability ($|r| =$

Table 2
Correlations between image textures vs. lidar- and field-based heterogeneity metrics, including standard deviation (SD) of lidar-based canopy height and nine field-based metrics: SD field-based vegetation height, Shannon diversity index (SDI) of foliage height, SD tree stem diameter, total basal area, cover SDI, and proportions of grass, herbaceous, shrub, and tree cover. Strongest correlations between lidar- and field-based metrics and textures at both 30 and 10 m resolutions, shown in bold. Note that two second-order textures, homogeneity and uniformity, quantify image *homogeneity*, thus a negative relationship between vegetation metrics and these textures represents a positive relationship with spatial *heterogeneity* of vegetation.

	SD Lidar canopy ht.	SD Field veg. ht.	Foliage ht. SDI	Basal area	SD Stem diam.	Cover SDI	% Grass cover	% Herb. cover	% Shrub cover	% Tree cover
30 m textures (Landsat 8):										
Std Dev	0.53	0.24	0.21	0.04	0.20	0.15	0.04	0.07	−0.01	0.05
Variance	0.53	0.15	0.15	0.04	0.15	0.06	0.02	0.02	0.03	0.05
Contrast	0.50	0.20	0.20	0.02	0.21	0.15	0.00	0.02	−0.04	**0.13**
Dissimilarity	0.53	0.31	0.25	0.03	0.25	0.20	0.06	0.08	−0.05	**0.13**
Homogeneity	**−0.64**	**−0.44**	**−0.31**	−0.07	**−0.34**	**−0.25**	**−0.11**	−0.16	0.09	−0.07
Entropy	0.61	0.41	0.29	0.07	0.30	0.24	0.10	0.15	−0.06	0.07
Uniformity	**−0.64**	−0.42	−0.30	**−0.08**	−0.31	−0.22	−0.06	**−0.17**	0.04	−0.07
Sum variance	0.53	0.14	0.15	0.04	0.14	0.05	0.02	0.02	0.04	0.05
Sum entropy	0.57	0.35	0.26	0.05	0.24	0.22	0.10	0.13	−0.03	0.06
Diff. variance	0.48	0.16	0.18	0.01	0.19	0.14	−0.03	0.00	−0.04	0.11
Diff. entropy	0.55	0.36	0.27	0.03	0.28	0.23	0.07	0.11	−0.05	0.11
Correlation	0.31	0.12	0.05	0.04	0.05	0.09	0.09	0.13	0.02	−0.07
Info. corr. 1	0.03	0.07	0.00	0.05	0.11	−0.01	0.00	0.05	**−0.12**	−0.02
Info. corr. 2	0.42	0.20	0.16	0.02	0.11	0.18	0.07	0.07	0.03	0.04
Cluster prominence	0.53	0.15	0.14	0.07	0.18	−0.07	−0.06	−0.03	0.04	−0.02
Cluster shade	−0.12	−0.13	−0.13	−0.05	−0.22	0.04	0.08	0.01	−0.02	0.02
10 m textures (Sentinel-2):										
Std Dev	0.55	0.20	0.25	0.06	0.25	0.10	0.05	−0.02	−0.18	0.06
Variance	0.55	0.09	0.18	0.05	0.21	−0.01	0.01	−0.08	−0.16	0.09
Contrast	0.71	0.35	0.33	0.12	0.46	0.13	−0.09	0.13	−0.31	0.03
Dissimilarity	0.75	0.45	0.36	0.15	0.50	0.18	−0.05	0.21	−0.34	−0.01
Homogeneity	**−0.80**	**−0.51**	**−0.36**	**−0.17**	**−0.52**	**−0.22**	−0.02	−0.26	0.35	0.06
Entropy	0.69	0.40	0.32	0.10	0.38	0.19	0.07	0.18	−0.23	−0.01
Uniformity	−0.72	−0.40	−0.25	−0.05	−0.35	−0.21	−0.12	−0.22	0.22	0.04
Sum variance	0.54	0.08	0.17	0.04	0.20	−0.01	0.01	−0.09	−0.15	0.09
Sum entropy	0.57	0.30	0.28	0.05	0.25	0.15	0.11	0.09	−0.13	0.03
Diff. variance	0.67	0.30	0.30	0.09	0.42	0.14	−0.09	0.07	−0.29	0.03
Diff. entropy	0.75	0.47	0.35	0.15	0.50	0.21	0.00	0.24	−0.34	−0.02
Correlation	0.09	−0.13	0.02	−0.09	−0.22	0.03	**0.16**	−0.23	0.23	0.09
Info. corr. 1	0.37	0.40	0.16	0.21	0.50	0.14	−0.11	**0.34**	**−0.40**	**−0.16**
Info. corr. 2	0.11	−0.12	0.04	−0.11	−0.24	0.02	**0.16**	−0.22	0.25	0.13
Cluster prominence	0.55	0.05	0.12	0.05	0.21	−0.03	−0.07	−0.12	−0.16	0.07
Cluster shade	−0.15	−0.03	−0.12	−0.03	−0.22	0.03	0.13	0.08	0.18	−0.10

0.64 and 0.80, respectively), followed by moderate correlations with several field-based measures of vegetation structure, including SD of vegetation height ($|r| \leq 0.51$) and tree stem diameter ($|r| \leq 0.52$), and – to a lesser degree – foliage height diversity ($|r| \leq 0.36$). Texture metrics such as homogeneity and information measure of correlation 1 were also correlated with plant compositional metrics, such as cover type diversity ($|r| \leq 0.25$), percent cover of shrubs ($|r| \leq 0.40$) and herbaceous plants ($|r| \leq 0.34$) at both 30 and 10 m resolutions. However, texture metrics were generally more strongly correlated with structural measures of vegetation heterogeneity than compositional measures.

EVI-based image texture captured distinct patterns of vegetation heterogeneity among the major habitat types we evaluated (i.e., forests, grasslands, shrublands; Fig. 3). In general, forests had highest EVI values and were more heterogeneous than grasslands, while shrublands tended to have lowest EVI values and were more homogeneous than either forests or grasslands. Forests and grasslands also had higher randomness in spatial distribution of vegetation than shrublands, characterized by entropy (Fig. 3f), whereas grassland and shrubland vegetation had higher spatial symmetry than forests, captured by cluster shade (Fig. 3h). Texture metrics captured high spatial variability of vegetation in drainage areas, particularly first-order standard deviation and second-order contrast (Fig. 3c, d) which highlighted marked differences in vegetation growth and human development in riparian areas relative to surrounding landscapes.

Image texture also characterized within-habitat heterogeneity of vegetation. For example, in the arid southwestern US (Fig. 3, right column), second-order homogeneity, entropy and information measure of correlation 1 captured substantial variability within a shrub-scrub dominated landscape, both in the Las Uvas Mountains west of the Rio Grande floodplain and in surrounding basins and playas (Fig. 3e–g). This likely reflects the ability of these texture metrics to characterize multiple components of vegetation heterogeneity within a single land cover type (Table 2).

We observed strong correlations among many texture metrics, particularly among texture groups that quantify similar elements of image heterogeneity. For example, Spearman's correlation coefficients among texture metrics of image contrast (i.e., contrast, dissimilarity, homogeneity) and image orderliness (i.e., uniformity, entropy, difference entropy) ranged from $|r| = 0.92–1.0$ (Figs. S4, S5). In general, texture metrics from the descriptive statistics group (i.e., correlation, information measures of correlation) were less correlated with metrics from the contrast and orderliness texture groups.

We also found positive correlations between 30 and 10 m resolution texture metrics, but some were surprisingly low ($|r| = 0.46–0.94$). Although texture metrics at both resolutions captured similar overall patterns of vegetation heterogeneity, 10 m texture metrics captured more details and finer-resolution features than 30 m resolution texture metrics (Figs. 2d-e, S6). Accordingly, 10 m resolution texture metrics were more strongly correlated with lidar- and field-based metrics than 30 m resolution texture metrics (Table 2).

3.2. Univariate bird richness models

Consistent with our predictions, both 30 and 10 m resolution texture metrics had higher explanatory power in univariate models of total bird richness than field-based vegetation metrics, explaining up to 31% and 45% of the variance in total bird richness, respectively, whereas field-based metrics only explained up to 14% (Table 3). Contrary to our predictions, some texture metrics also outperformed lidar-based canopy height variability, which explained 25% of the variance in total bird richness. Of all the individual predictors we evaluated, 10 m resolution homogeneity texture had the highest explanatory power (45% of variance explained) followed closely by 10 m resolution dissimilarity (44%) and difference entropy (44%) textures. However, we observed considerable variability in the relationships between different texture metrics and richness of habitat specialists in forest, grassland, and shrubland areas. NEON lidar canopy height data and field-based measures of vegetation structure were limited in grassland and shrubland habitats, and the relationships between texture and bird richness that were statistically significant but had relatively low R^2 values should be interpreted with caution. In general, texture metrics were positively related with richness of all birds combined and of forest specialists but were non-significant or weak predictors of grassland bird richness, and negatively related with shrubland specialist richness (Table 3).

In univariate models of forest specialist richness, SD of field-based vegetation height (25% of variance explained) and total basal area (17%) were the strongest predictors, followed by the 10 m resolution homogeneity texture (16%; Table 3). Conversely, 30 m resolution cluster shade texture was the strongest individual predictor of grassland specialist richness (13%), and no field-based vegetation metrics were significant in univariate models for grassland specialists. Percent grass cover was not positively related with grassland specialist richness, suggesting there may not have been sufficient variability in grass cover at the scale of measurements to detect a relationship with bird richness, or that grassland specialists are responding to specific habitat features not included in our analysis. Shrubland specialist richness was best explained by 10 m resolution information measure of correlation 1 (45%) and 30 m resolution entropy (32%) textures, and poorly explained by lidar canopy height variability and field-based measures. Overall, texture metrics had the highest explanatory power for all birds combined and shrubland specialists, field-based measures of vegetation structural heterogeneity were the best predictors of forest specialist richness, and all predictors had relatively low explanatory power for grassland specialists.

3.3. Relative importance of textures

We inlcuded six metrics in our multivariate models based on results of our exploratory correlation analyses and univariate models. We selected the homogeneity texture metric because it had the strongest relationship with total bird richness at both 30 and 10 m resolutions and because it is highly correlated with other texture metrics that were also good predictors of bird richness (e.g., dissimilarity and entropy; Table 3; Figs. S4, S5). We selected two additional texture metrics, information measure of correlation 1 and cluster shade texture, because they were relatively uncorrelated with homogeneity and had stronger relationships with grassland and shrubland specialists (Table 3). We included SD of lidar-based canopy height because it performed well in bird richness models. This was the only lidar-based metric we evaluated. Lastly, we included SD of field-based vegetation height and plant cover type SDI. Although plant cover type SDI was not a strong predictor in univariate models, we included it as a representative measure of vegetation compositional heterogeneity that was not highly correlated with structural measures of lidar-based canopy height or field-based vegetation height ($|r| = 0.30–0.41$; Fig. S1). SD of lidar-based canopy height had the two highest correlations with SD of field-based vegetation height ($|r| = 0.79$) and 10 m resolution homogeneity ($|r| = 0.73$). However, these were three predictors of primary interest and correlations among other predictors were relatively low (mean $|r| = 0.24$), thus we chose to retain all six predictors in our multivariate model sets.

The top model of total bird richness that included 10 m resolution texture metrics explained 55% of the variance in total bird richness and contained only two texture metrics: homogeneity and information measure of correlation 1 (Table 4). The same two texture metrics were selected in the top-ranked model with 30 m resolution texture metrics, in addition to lidar-based canopy height variability, which together explained 42% of the variance in total bird richness. In models containing both 10 and 30 m resolution texture metrics, the homogeneity texture had the largest effect size and a negative effect on total bird richness (Fig. 4). Homogeneity also had the largest independent contribution towards variance explained in models of total bird richness (Fig. 5). Again, these results should be interpreted with caution, given

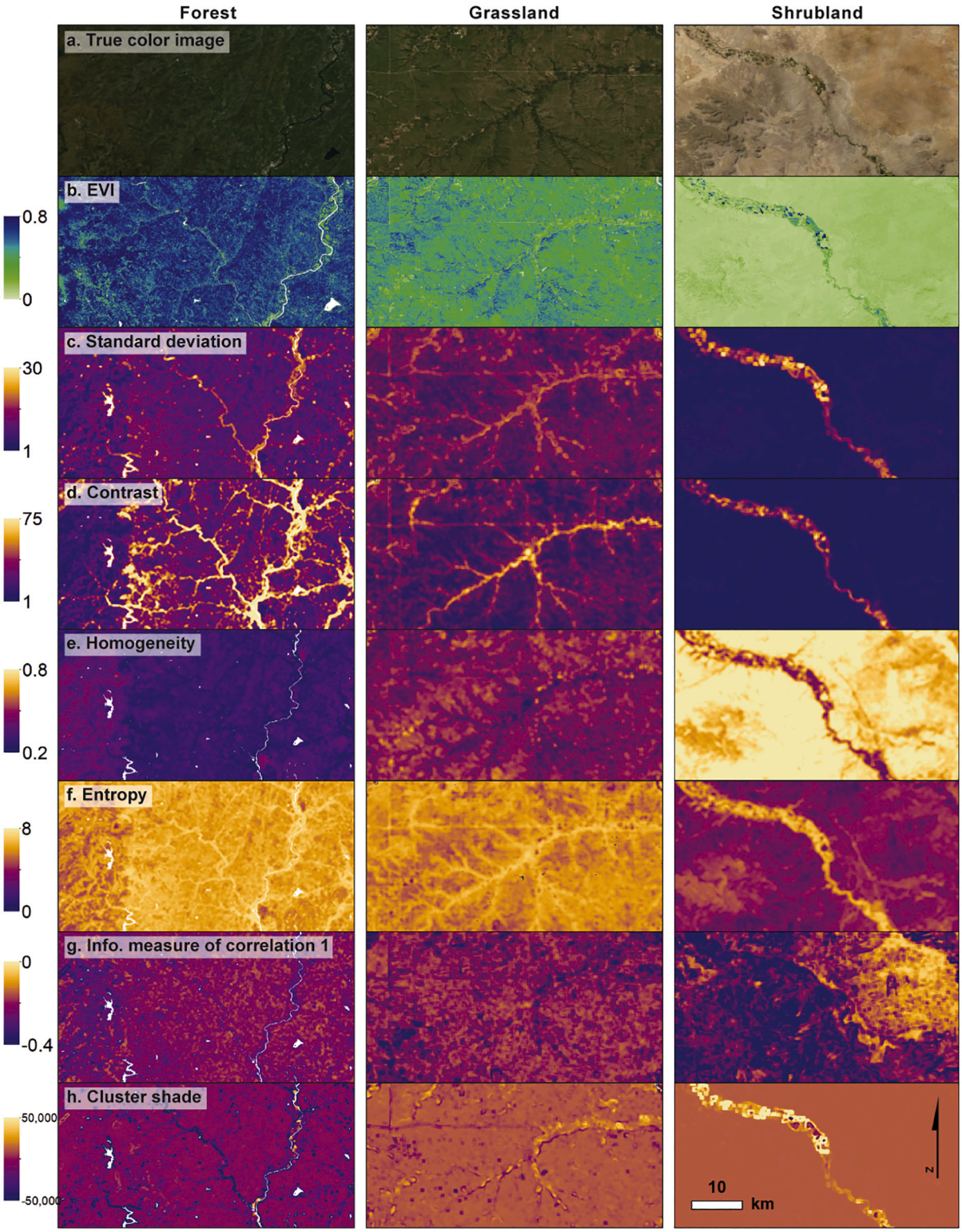

Fig. 3. True color images (a) and examples of vegetation heterogeneity captured by enhanced vegetation index (EVI; b) and texture metrics derived from 10 m resolution Sentinel-2 imagery (c-h), within landscapes representing forest, grassland, and shrubland habitats: (1) mixed evergreen-deciduous forest near the Harvard Forest site in the northeastern US (43°0′16″ N, 72°39′57″ W); (2) tallgrass prairie in the Flint Hills of Kansas near the Konza Prairie Biological Station (39°0′43″ N, 96°18′43″ W); and (3) shrubland in the Chihuahuan Desert near the Jornada Long Term Ecological Research site, in southwestern US (32°35′1″ N, 107°0′59″ W). All three featured landscapes are located close to NEON sites we evaluated (within 15–65 km) and were selected to highlight differences among texture metrics visible at a broader spatial extent (30 × 50 km = 150,000 ha) than inidividual NEON plots (750 × 750 m = 56.25 ha). The texture metrics featured here represent main types of texture metrics (Hall-Beyer, 2017), are relatively uncorrelated, and include the texture metrics in our multivariate analyses.

Table 3
Results of univariate linear regression models showing relationships between lidar, field, and texture metrics, and richness of all bird species combined ($n = 329$) and forest ($n = 75$), grassland ($n = 14$), and shrubland specialists ($n = 27$). For each set of predictors and species group, models with the highest adjusted R^2 values are shown in bold. Non-significant models ($p < 0.05$) are indicated with dashes. Note that two second-order textures, homogeneity and uniformity, quantify image *homogeneity*, thus a negative relationship between bird richness and these textures represents a positive relationship with spatial *heterogeneity* of vegetation.

	All bird species		Forest specialists		Grassland specialists		Shrubland specialists	
	Est.	R^2_{adj}	Est.	R^2_{adj}	Est.	R^2_{adj}	Est.	R^2_{adj}
Lidar-based metric:								
SD Lidar canopy ht.	5.93	**0.25**	1.71	0.11	0.48	**0.10**	–	–
Field-based metrics:								
SD Vegetation ht.	4.32	0.13	2.52	**0.25**	–	–	–	–
Foliage ht. SDI	3.80	0.10	1.77	0.12	–	–	–	–
SD Tree stem diam.	4.43	0.14	1.89	0.14	–	–	–	–
Total basal area	3.26	0.07	2.06	0.17	–	–	–	–
Cover SDI	2.64	0.05	–	–	–	–	–	–
% Grass cover	1.55	0.01	−1.13	0.04	–	–	–	–
% Herb. cover	3.64	0.09	–	–	–	–	–	–
% Shrub cover	−4.26	0.13	–	–	–	–	–	–
% Tree cover	–	–	–	–	–	–	−0.91	**0.09**
30 m textures (Landsat 8):								
Std Dev	4.55	0.15	–	–	–	–	−1.26	0.19
Variance	3.15	0.07	–	–	–	–	−0.84	0.07
Contrast	4.39	0.13	–	–	–	–	−0.87	0.08
Dissimilarity	5.95	0.25	1.29	0.06	–	–	−1.30	0.21
Homogeneity	−6.58	**0.31**	−1.74	0.12	–	–	1.55	0.30
Entropy	5.96	0.25	1.61	0.10	–	–	−1.59	**0.32**
Uniformity	−4.34	0.13	−1.82	**0.13**	–	–	1.25	0.19
Sum variance	2.97	0.06	–	–	–	–	−0.83	0.07
Sum entropy	5.42	0.21	1.30	0.06	–	–	−1.56	0.30
Diff. variance	3.60	0.09	–	–	–	–	−0.79	0.06
Diff. entropy	6.22	0.27	1.52	0.09	–	–	−1.50	0.28
Correlation	–	–	–	–	–	–	–	–
Info. corr. 1	3.16	0.07	–	–	0.47	0.09	–	–
Info. corr. 2	3.21	0.07	–	–	–	–	−1.42	0.25
Prominence	1.92	0.02	–	–	–	–	–	–
Shade	–	–	–	–	0.54	**0.13**	–	–
10 m textures (Sentinel-2):								
Std Dev	5.44	0.21	–	–	–	–	−1.02	0.12
Variance	3.71	0.09	–	–	–	–	−0.76	0.06
Contrast	7.10	0.36	1.32	0.06	–	–	–	–
Dissimilarity	7.87	0.44	1.71	0.11	–	–	−0.89	0.09
Homogeneity	−7.96	**0.45**	−2.01	**0.16**	−0.43	0.07	0.88	0.08
Entropy	6.93	0.34	1.47	0.08	–	–	−1.15	0.16
Uniformity	−4.67	0.15	−1.57	0.09	–	–	0.78	0.06
Sum variance	3.52	0.08	–	–	–	–	−0.76	0.06
Sum entropy	6.10	0.26	1.00	0.03	–	–	−1.24	0.19
Diff. variance	6.69	0.32	1.06	0.04	–	–	–	–
Diff. entropy	7.88	0.44	1.75	0.12	–	–	−0.94	0.10
Correlation	–	–	–	–	–	–	−1.42	0.25
Info. corr. 1	5.40	0.21	1.88	0.14	0.48	**0.10**	1.87	**0.45**
Info. corr. 2	1.98	0.02	–	–	–	–	−1.58	0.31
Prominence	1.91	0.02	–	–	–	–	–	–
Shade	−1.70	0.02	–	–	0.49	**0.10**	–	–

the limited availability of lidar canopy height data and field-based measurements of vegetation structure in NEON sites dominated by grasslands, and to a lesser extent shrublands. Still, these results are consistent with our prediction that texture would contribute independent explanatory power in multivariate models and indicates that image texture not only complements more common metrics of vegetation heterogeneity in models of bird richness, but in some cases may outperform them.

Among forest specialists, top-ranked models including 30 and 10 m resolution texture metrics had similar explanatory power (32% and 33%, respectively) and included field-based vegetation height variability, plant cover type diversity, and homogeneity texture (Table 4). In both models, field-based vegetation height variability had the strongest effect (Fig. 4) and contributed the most independent explanatory power (Fig. 5). For grassland specialists, top-ranked models containing 30 and 10 m resolution texture metrics also explained similar variance in richness (29% and 26%, respectively), but included only texture metrics (Table 4). For shrubland specialist richness, top-ranked models constructed at both resolutions included only one texture predictor: 30 m resolution homogeneity explained 32% of the variance in shrubland specialist richness, while 10 m resolution information measure of correlation 1 explained 46% of the variance.

For all species groups evaluated, variance inflation factors (VIFs) for predictors in top-ranked models were < 1.5 (mean VIF = 1.17; Table S5), indicating negligible levels of multicollinearity (Booth et al., 1994). In spline correlograms, Moran's *I* is estimated with cubic splines as a continuous function of distance and 95% confidence intervals are generated using a bootstrap approach, such that evidence for spatial dependence is significant when confidence intervals do not overlap zero (Bjornstad and Falck, 2001). Our confidence intervals for spline correlograms of model residuals of total bird richness among survey plots suggested some spatial autocorrelation at shorter lag distances, which may have tightened our confidence limits (e.g., Fig. 4) but spatial autocorrelation does not affect model coefficients or marginal effects,

Table 4
Competing models of bird richness ranked by Bayesian information criterion (BIC). Results are shown for top-ranked models and models with ΔBIC <2, for all species combined ($n = 329$) and forest ($n = 75$), grassland ($n = 14$), and shrubland specialists ($n = 27$). Models shown in (a) included 30 m resolution textures, and in (b) included 10 m resolution textures. Predictor abbreviations: intercept (Int.), standard deviation of lidar-based canopy height (SD Lidar canopy ht.) and field-based vegetation height (SD Veg. ht.), Shannon diversity index of plant cover (Cover SDI), information measure of correlation 1 (Info. corr. 1), and cluster shade (Shade). Adjusted R^2 values in bold for top-ranked model in each group; predictors not included in top models are indicated by dashes.

(a) 30 m texture models (Landsat 8):

	Mod. rank	Int.	SD Lidar canopy ht.	SD Veg. ht.	Cover SDI	Homo-geneity	Info. corr. 1	Shade	df	logLik	BIC	ΔBIC	Wt.	R^2_{adj}
All	1	26.50	3.04	–	–	−4.75	2.77	–	5	−806.3	1639.6	0.00	0.79	**0.42**
Forest	1	14.44	–	2.17	−1.04	−1.02	–	–	5	−310.1	643.8	0.00	0.22	**0.32**
	2	14.44	–	2.52	–	–	–	–	3	−314.8	643.8	0.04	0.22	0.26
	3	14.44	–	2.60	−0.84	–	–	–	4	−312.7	644.2	0.46	0.18	0.29
	4	14.44	0.97	2.14	−1.10	–	–	–	5	−310.7	644.9	1.15	0.12	0.31
	5	14.44	–	2.18	–	−0.77	–	–	4	−313.4	645.6	1.83	0.09	0.28
Grass	1	2.43	–	–	–	–	0.53	0.59	4	−74.5	164.4	0.00	0.32	**0.29**
	2	2.43	–	–	–	−0.33	0.51	0.57	5	−72.6	164.5	0.08	0.31	0.35
Shrub	1	1.90	–	–	–	1.55	–	–	3	−116.4	244.6	0.00	0.44	**0.32**

(b) 10 m texture models (Sentinel-2):

	Mod. rank	Int.	SD Lidar canopy ht.	SD Veg. ht.	Cover SDI	Homo-geneity	Info. corr. 1	Shade	df	logLik	BIC	ΔBIC	Wt.	R^2_{adj}
All	1	26.50	–	–	–	−7.06	3.65	–	4	−778.6	1578.8	0.00	0.64	**0.55**
Forest	1	14.44	–	2.03	−1.01	−1.22	–	–	5	−309.1	641.8	0.00	0.23	**0.33**
	2	14.44	–	2.18	−0.90	–	1.10	–	5	−309.4	642.3	0.59	0.17	0.33
	3	14.44	–	2.11	–	–	1.04	–	4	−312.0	642.8	1.08	0.13	0.30
	4	14.44	–	1.86	−1.01	−0.92	0.79	–	6	−307.5	643.3	1.54	0.11	0.35
	5	14.44	–	2.02	–	−1.03	–	–	4	−312.4	643.5	1.75	0.09	0.29
Grass	1	2.43	–	–	–	−0.51	–	0.56	4	−75.6	166.6	0.00	0.31	**0.26**
	2	2.43	–	–	–	−0.43	0.30	0.51	5	−74.4	168.0	1.32	0.16	0.30
	3	2.43	–	–	0.25	−0.49	–	0.57	5	−74.6	168.5	1.84	0.12	0.29
Shrub	1	1.90	–	–	–	–	1.88	–	3	−110.2	232.3	0.00	0.40	**0.46**
	2	1.90	−0.42	–	–	–	1.80	–	4	−109.1	234.1	1.72	0.17	0.49

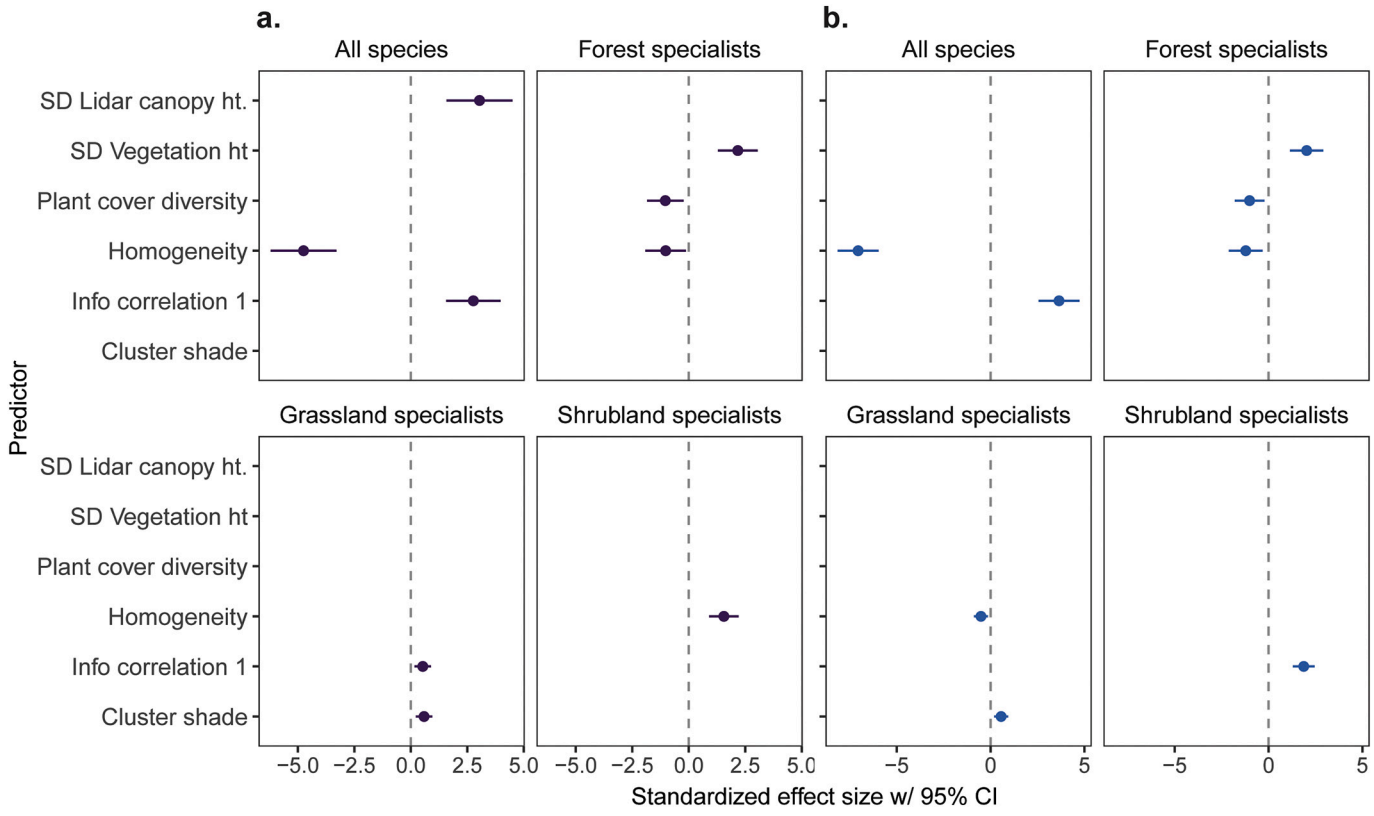

Fig. 4. Standardized regression coefficients are shown for predictors in top bird richness models for four species groups, as measures of effect size (with 95% confidence intervals). Results are shown for models that included (a) 30 m resolution (Landsat 8) and (b) 10 m resolution (Sentinel-2) EVI textures.

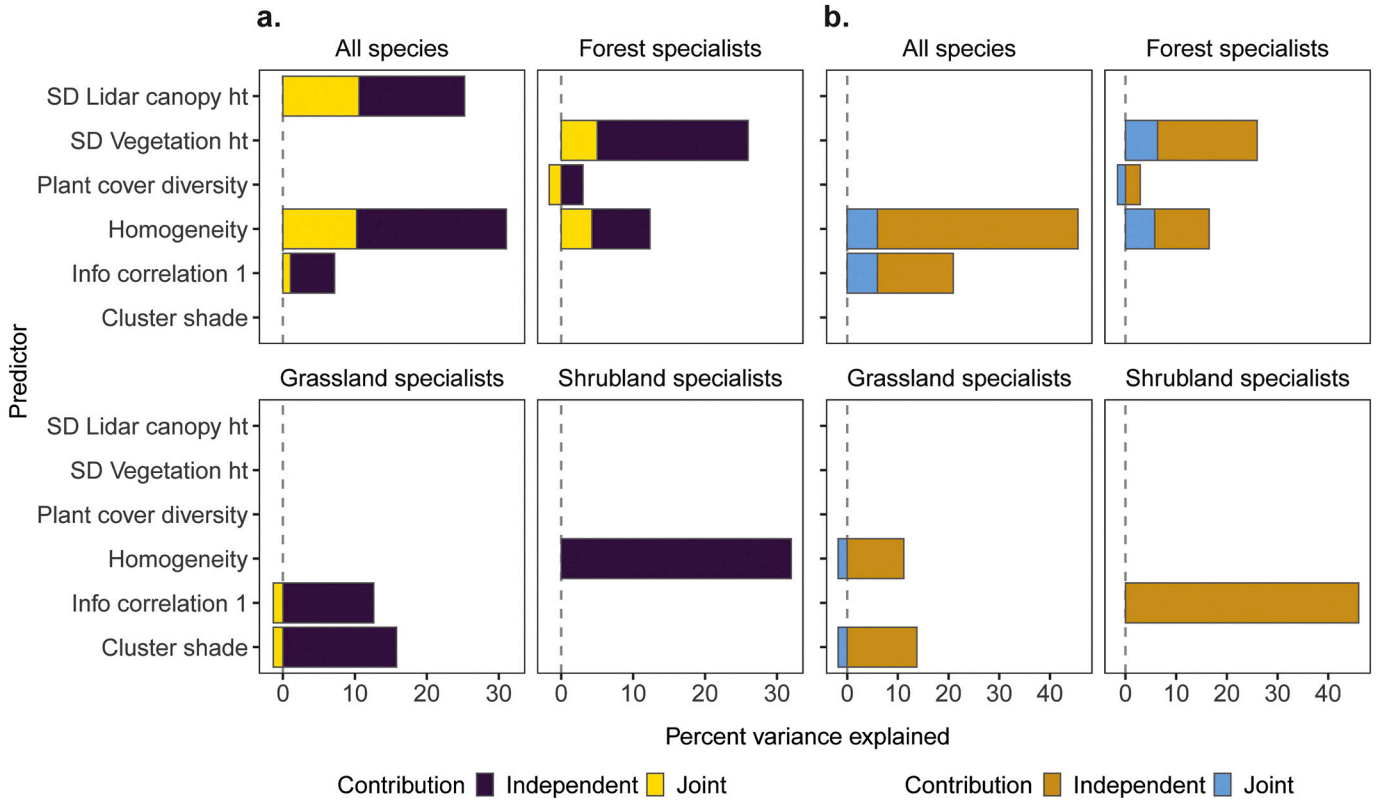

Fig. 5. Relative influence of predictors in top bird richness models for four species groups, as measured by independent and joint contributions from hierarchical partitioning. Results are shown for models that included (a) 30 m resolution (Landsat 8) and (b) 10 m resolution (Sentinel-2) EVI textures. Note that top models for shrubland specialists included only one predictor (independent contribution only).

which we focused on when evaluating our models (Fig. S7; Fletcher and Fortin, 2018).

4. Discussion

We linked image texture with localized vegetation attributes in landscapes across the continental US and found that satellite image texture captured multiple components of vegetation heterogeneity that influence species richness patterns, across a range of ecosystems. In general, image texture was more strongly correlated with measures of vegetation structure than composition, particularly measures of vertical vegetation structure. However, texture was also correlated with some elements of plant compositional diversity. In models of bird richness, we found that texture complemented both lidar-based canopy height variability and field-based metrics of vegetation heterogeneity, and showed an even stronger relationship with patterns of bird richness for some guilds.

4.1. Texture characterization of vegetation heterogeneity

Image texture was positively correlated with several different features of vegetation heterogeneity. At both 30 and 10 m resolutions, texture metrics were most strongly correlated with lidar-based canopy height variability, followed by SD of field measured vegetation height and tree stem diameter, and foliage height diversity. These are all related measures of structural heterogeneity that characterize different elements of vegetation configuration in three-dimensions (O'Brien et al., 1995). We found that image texture was most strongly related to vertical complexity of plant structure but was also weakly to moderately correlated with compositional heterogeneity measures, such as plant cover type diversity and percent shrub and herbaceous cover. This suggests satellite image texture may offer the advantage of characterizing vegetation structural complexity while also providing ancillary information about plant compositional heterogeneity. In many environments, plants form the physical structure of habitats and thus have a strong effect on species richness patterns (McCoy and Bell, 1991). However, both the structural and compositional heterogeneity of vegetation can increase available niche space and are important determinants of species distributions and diversity (Lee and Rotenberry, 2005; Schuldt et al., 2019).

Measurements of heterogeneity depend on the spatial resolution of imagery (Rocchini, 2007; Gillespie et al., 2008). Coarse-resolution satellite images often have mixed pixels when features of interest are smaller than the resolution of the image (Foody and Cox, 1994). Image texture metrics at the two resolutions we evaluated were correlated and had similar relationships with lidar- and field-based vegetation metrics. However, 10 m resolution texture metrics were generally more strongly correlated with lidar- and field-based metrics than 30 m texture metrics, suggesting image texture derived from 10 m resolution Sentinel-2 imagery is better able to characterize vegetation features of interest. Our findings are consistent with other studies evaluating these spatial resolutions for mapping vegetation characteristics. For example, vegetation metrics based on Sentinel-2 imagery outperformed metrics based on Landsat 8 imagery in quantifying structural diversity of high-elevation forests (Morley et al., 2019), and Sentinel-2 data were better predictors of field-based vegetation metrics than data from Landsat 8 in a boreal forest (Astola et al., 2019).

4.2. Texture and bird richness

We also found that several texture metrics derived from 30 and 10 m resolution imagery had strong relationships with bird richness. Texture metrics had higher explanatory power than field-based metrics in univariate models of total bird richness, which may partly reflect the

continuous measures of vegetation heterogeneity that image texture provides across landscapes, whereas field-based metrics are derived from data sampled over limited spatial extents (Rocchini et al., 2010). Bird richness may also have been more strongly related to texture in univariate models because individual texture metrics captured multiple facets of vegetation complexity, and bird-habitat relationships are complex and influenced by both vegetation structure and composition (Rotenberry, 1985; Skowno and Bond, 2003). Univariate model results should be interpreted with caution, however, because field-based metrics of vegetation structure and composition can be combined in multivariate models to increase explanatory power (e.g., Table 4). Similarly, some texture metrics were also stronger predictors of total bird richness than lidar-based canopy height variability. This contradicted our prediction that texture metrics and lidar canopy height variability would have comparable explanatory power in bird richness models. Yet, 2.5 m resolution satellite image texture also has similar or higher explanatory power than lidar-derived vertical structure metrics in models of bird diversity in an Ecuadorian rainforest (Wallis et al., 2016), and 30 m texture metrics outperform both field-measured vegetation structure and 1 m resolution air photo textures in models of bird richness in grassland, savanna, and woodland habitats in the Midwestern US (Wood et al., 2013). Our findings are consistent with these prior studies, and demonstrate the utility of texture metrics derived from medium-resolution satellite imagery for modeling bird richness.

Just as spatial resolution affects the ability of imagery to capture vegetation characteristics, resolution can also influence the relationship between vegetation heterogeneity and biodiversity (Bar-Massada et al., 2012) and may have influenced differences we observed among habitats evaluated. Broadly, our findings demonstrate that 10 to 30 m resolution image texture characterizes spatial heterogeneity of vegetation that influences overall bird richness across different habitats, as well as richness of specialists within forests and shrublands. However, these spatial resolutions may be too coarse to effectively capture finer-resolution features within grasslands (Ali et al., 2016), particularly microhabitat variations that are important for birds such as fine-scale vegetation height and density, litter cover and depth, and amount of bare ground and dead vegetation (Fisher and Davis, 2010; Jacobs et al., 2012). It is possible that textures calculated from higher resolution imagery (e.g., Lussem et al., 2019) or the integration of field-data and remotely sensed metrics (Ali et al., 2016) can better characterize these fine-scale features of grassland heterogeneity.

We also found that 10 m resolution texture consistently outperformed 30 m resolution texture in bird richness models, most likely because 10 m resolution texture more effectively captured multiple features of vegetation complexity known to influence bird communities (Rotenberry, 1985; Skowno and Bond, 2003). This result is consistent with previous findings that vegetation metrics based on finer resolution imagery (2–5 m) outperform those derived from coarser resolution imagery (10–250 m) in bird richness models of both farmland-woodland (Sheeren et al., 2014) and forest landscapes (Ozdemir et al., 2018), although 10 m indices perform almost as well in both landscapes. However, higher resolution metrics do not always show stronger relationships with biodiversity patterns, especially when vegetation features are larger than the pixel resolution (Nagendra and Rocchini, 2008). Given the discrepancy in predictive power of texture that we observed among habitat types, we suggest that both the spatial resolution of imagery and the extent of analysis (i.e., sampling units and moving window size) should be carefully chosen to ensure patterns of interest are captured at scales relevant for the taxa of interest.

In univariate models at both resolutions we evaluated, the individual texture with the highest explanatory power for total bird richness was homogeneity, followed closely by dissimilarity and entropy. This finding is consistent with previous studies that used image texture to model bird richness (Culbert et al., 2012; Tuanmu and Jetz, 2015; Farwell et al., 2020). Homogeneity quantifies the smoothness of an image, with high values indicating an absence of feature complexity and locally even distribution of image features (Hall-Beyer, 2017). Dissimilarity quantifies image contrast, with higher values reflecting sharp differences among neighboring features. Entropy quantifies image non-uniformity, with higher values reflecting randomness in the distribution of image features. We found that these texture metrics were highly correlated, similar to others (St-Louis et al., 2006; Culbert et al., 2012; Farwell et al., 2020). Thus, although the four texture metrics that had the highest explanatory power for total bird richness may capture slightly different aspects of image contrast and orderliness (i.e., homogeneity, dissimilarity, entropy, difference entropy), we suggest that a single representative texture metric of image contrast or orderliness may be sufficient to capture a range of vegetation heterogeneity features that are important for species.

When we evaluated multivariate models of bird richness that combined texture metrics, lidar canopy height variability and field-based measurements, we found that texture metrics complemented the other more commonly used vegetation metrics and in some cases outperformed our other predictors. Texture had significant associations with patterns of bird richness and contributed the most independent explanatory power in several multivariate models. This may partly reflect limitations of the NEON lidar canopy height data and field-based measures of vegetation structure in grassland and shrubland habitats. However, this may also reflect the wall-to-wall coverage provided by satellite image texture, in addition to our finding that texture metrics are able to capture multifaceted complexity of vegetation structure and composition. These may be important advantages of using texture metrics in combination with field-based metrics with limited spatial coverage and/or lidar-based measures which primarily characterize three-dimensional structure of vegetation (Davies and Asner, 2014; Vogeler et al., 2014). However, we acknowledge that in our model selection framework, the top-ranked model for each bird group is only the best model relative to the limited number of models and predictors considered. Still, our results were consistent across image resolutions, habitat types, and bird groups and highlight cases in which textures can be used to improve biodiversity models.

4.3. Caveats and considerations

It is important to keep several caveats related to the NEON data in mind when interpreting these results. First, the exclusion of vegetation <2 m tall from the lidar canopy height model provided by NEON resulted in limited canopy height data in grassland habitats, and to a lesser extent in shrubland habitats. This likely contributed to the relatively poor performance of our lidar-based canopy height variability metric in models of bird richness. However, in models of forest specialist richness that focused on forest-dominated landscapes with ample NEON lidar canopy height data, image texture still outperformed lidar-based canopy height variability. Additionally, even in grassland and shrubland habitats with limited lidar data, image texture alone explained 26–29% of the variance in grassland specialist richness, and 32–46% of the variance in shrubland specialist richness.

Second, there were limitations in the NEON field measures of vegetation. Structural metrics were only available for woody vegetation, resulting in limited field data for habitats dominated by grass and herbaceous vegetation. Additionally, we had to derive vegetation compositional heterogeneity from plant presence and percent cover (PPPC) data collected in 1 m^2 plots, representing a very limited spatial extent. It is possible that more comprehensive plant cover and species data might have improved the performance of compositional metrics in models of bird richness. Nevertheless, the vegetation sampling approach used by NEON is standardized for various features of vegetation heterogeneity (Barnett et al., 2019b), and thus were appropriate for comparison with EVI-based image textures. Lastly, while we could have evaluated additional lidar- and field-based metrics, our intention here was to compare the performance of image texture with other readily available,

commonly used measures of vegetation heterogeneity.

4.4. Conclusions and conservation implications

By linking image texture directly with both lidar- and field-based vegetation measures and bird richness, we demonstrate that satellite image texture captures multiple components of vegetation heterogeneity that are important for explaining biodiversity patterns. We found that texture was strongly correlated with measures of vegetation structural complexity, but also provided information about plant compositional heterogeneity. We suggest this helps to explain why image texture based on either 10 or 30 m resolution satellite data performed quite well in our models of bird species richness. This has important conservation implications because species distributions and diversity are influenced by the heterogeneity of both vegetation structure and composition. Our results indicate that textures are not just easy-to-obtain surrogates for lidar- and field-based measures of vegetation complexity, but are complementary and strong predictors of species richness, in their own right. Notably, we found that a single second-order texture measure (e.g., homogeneity, dissimilarity, or entropy) may be sufficient to significantly improve biodiversity models. Image resolution is important though, and we found that 10 m Sentinel-2 image texture clearly outperformed 30 m Landsat texture. Our findings are important because advances in cloud computing for remote sensing data have increased the accessibility of satellite imagery and reduced the processing time for image texture calculations, making it possible to include 10–30 m resolution image textures for ecological applications at continental scales. We acknowledge the inherent challenge of managing a given landscape for "increased texture" (e.g., lower homogeneity), and the value of both lidar and field data when interpreting texture measures. In general, we suggest that texture metrics are best suited to identify and prioritize heterogeneous landscapes that already have high potential for supporting biodiversity, and to improve species distribution models and change projections. We recommend that future studies consider including image texture in biodiversity models, especially for species groups or taxa that are strongly associated with vegetation heterogeneity.

Declaration of Competing Interest

None.

Acknowledgements

This research was supported by the USGS Landsat Science Team (Grant Number 140G0118C0009), and by NASA's Biodiversity and Ecological Forecasting Program. The National Ecological Observatory Network is sponsored by the National Science Foundation and operated under a cooperative agreement by Battelle Memorial Institute. We thank the three anonymous reviewers who provided valuable comments that greatly improved this manuscript.

Appendix A. Supplementary data

Supplementary material can be found online at https://doi.org/10.1016/j.rse.2020.112175.

References

Ali, I., Cawkwell, F., Dwyer, E., Barrett, B., Green, S., 2016. Satellite remote sensing of grasslands: from observation to management. J. Plant Ecol. 9 (6), 649–671.
Astola, H., Hame, T., Sirro, L., Molinier, M., Kilpi, J., 2019. Comparison of Sentinel-2 and Landsat 8 imagery for forest variable prediction in boreal region. Remote Sens. Environ. 223, 257–273.
Baraldi, A., Parmiggiani, F., 1995. An investigation of the textural characteristics associated with gray-level co-occurrence matrix statistical parameters. IEEE Trans. Geosci. Remote Sens. 33 (2), 293–304.
Bar-Massada, A., Wood, E.M., Pidgeon, A.M., Radeloff, V.C., 2012. Complex effects of scale on the relationships of landscape pattern versus avian species richness and community structure in a woodland savanna mosaic. Ecography 35 (5), 393–411.
Barnett, D.T., Duffy, P.A., Schimel, D.S., Krauss, R.E., Irvine, K.M., Davis, F.W., Gross, J. E., Azuaje, E.I., Thorpe, A.S., Gudex-Cross, D., Patterson, M., McKay, J.M., McCorkel, J.T., Meier, C.L., 2019a. The terrestrial organism and biogeochemistry spatial sampling design for the National Ecological Observatory Network. Ecosphere 10 (2), 1–23.
Barnett, D.T., Adler, P.B., Chemel, B.R., Duffy, P.A., Enquist, B.J., Grace, J.B., Harrison, S., Peet, R.K., Schimel, D.S., Stohlgren, T.J., Vellend, M., 2019b. The plant diversity sampling design for the National Ecological Observatory Network. Ecosphere 10 (2), 1–18.
Barton, K., 2019. MuMIn: Multi-Model Inference. R Package Version 1.43.15. https://CRAN.R-project.org/package=MuMIn.
Bellis, L.M., Pidgeon, A.M., Radeloff, V.C., St-Louis, V., Navarro, J.L., Martella, M.B., 2008. Modeling habitat suitability for greater rheas based on satellite image texture. Ecol. Appl. 18 (8), 1956–1966.
Benton, T.G., Vickery, J.A., Wilson, J.D., 2003. Farmland biodiversity: is habitat heterogeneity the key? Trends Ecol. Evol. 18 (4), 182–188.
Billerman, S.M., Keeney, B.K., Rodewald, P.G., Schulenberg, T.S. (Eds.), 2020. Birds of the World. Cornell Laboratory of Ornithology, Ithaca, NY, USA. https://birdsoftheworld-org.ezproxy.library.wisc.edu/bow/home>.
Bjornstad, O.N., 2020. ncf: Spatial Covariance Functions. R Package Version 1.2-9. https://CRAN.R-project.org/package=ncf>.
Bjornstad, O.N., Falck, W., 2001. Nonparametric spatial covariance functions: estimation and testing. Environ. Ecol. Stat. 8 (1), 53–70.
Booth, G.D., Niccolucci, M.J., Schuster, E.G., 1994. Identifying proxy sets in multiple linear regression: An aid to better coefficient interpretation. In: Research Paper INT-470. U.S. Department of Agriculture, Forest Service, Intermountain Research Station, Ogden, Utah.
Brewer, M.J., Butler, A., Cooksley, S.L., 2016. The relative performance of AIC, AICc and BIC in the presence of unobserved heterogeneity. Methods Ecol. Evol. 7 (6), 679–692.
Briggs, J.M., Nellis, M.D., 1991. Seasonal variation of heterogeneity in the tallgrass prairie- a quantitative measure using remote sensing. Photogramm. Eng. Remote. Sens. 57 (4), 407–411.
Burnham, K.P., Anderson, D.R., 2004. Multimodel inference: understanding AIC and BIC in model selection. Sociol. Methods Res. 33 (2), 261–304.
Campos, V.E., Gatica, G.M., Cappa, F.M., Giannoni, S.M., Campos, C.M., 2018. Remote sensing data to assess compositional and structural indicators in dry woodland. Ecol. Indic. 88, 63–70.
Cardinale, B.J., Duffy, J.E., Gonzalez, A., Hooper, D.U., Perrings, C., Venail, P., Narwani, A., Mace, G.M., Tilman, D., Wardle, D.A., Kinzig, A.P., Daily, G.C., Loreau, M., Grace, J.B., Larigauderie, A., Srivastava, D.S., Naeem, S., 2012. Biodiversity loss and its impact on humanity. Nature 486 (7401), 59–67.
Castagneyrol, B., Jactel, H., 2012. Unraveling plant-animal diversity relationships: a meta-regression analysis. Ecology 93 (9), 2115–2124.
Chevan, A., Sutherland, M., 1991. Hierarchical partitioning. Am. Stat. 45 (2), 90–96.
Cody, M.L., 1968. On the methods of resource division in grassland bird communities. Am. Nat. 102 (924), 107–147.
Conners, R.W., Trivedi, M.M., Harlow, C.A., 1984. Segmentation of a high-resolution urban scene using texture operators. Comput. Vision Graph. Image Process. 25 (3), 273–310.
Creech, T.G., Epps, C.W., Monello, R.J., Wehausen, J.D., 2016. Predicting diet quality and genetic diversity of a desert-adapted ungulate with NDVI. J. Arid Environ. 127, 160–170.
Culbert, P.D., Radeloff, V.C., St-Louis, V., Flather, C.H., Rittenhouse, C.D., Albright, T.P., Pidgeon, A.M., 2012. Modeling broad-scale patterns of avian species richness across the Midwestern United States with measures of satellite image texture. Remote Sens. Environ. 118, 140–150.
Davies, A.B., Asner, G.P., 2014. Advances in animal ecology from 3D-LiDAR ecosystem mapping. Trends Ecol. Evol. 29 (12), 681–691.
Engemann, K., Sandel, B., Boyle, B., Enquist, B.J., Jorgensen, P.M., Kattge, J., McGill, B. J., Morueta-Holme, N., Peet, R.K., Spencer, N.J., Violle, C., Wiser, S.K., Svenning, J.-C., 2016. A plant growth form dataset for the New World. Ecology 97 (11), 3243.
ESRI [Environmental Research Systems Institute], 2016. ArcGIS Desktop: Release 10.5.1. Redlands, CA, USA.
Farwell, L.S., Elsen, P.R., Razenkova, E., Pidgeon, A.M., Radeloff, V.C., 2020. Habitat heterogeneity captured by 30 m resolution satellite image texture predicts bird richness across the U.S. In: Ecological Applications (in press).
Fisher, R.J., Davis, S.K., 2010. From Wiens to Robel: a review of grassland-bird habitat selection. J. Wildl. Manag. 74 (2), 265–273.
Fletcher, R., Fortin, M.-J., 2018. Spatial dependence and autocorrelation. In: Spatial Ecology and Conservation Modeling. Springer, Cham.
Foody, G.M., Cox, D.P., 1994. Sub-pixel land-cover composition estimation using a linear mixture model and fuzzy membership functions. Int. J. Remote Sens. 15 (3), 619–631.
Fox, J., Weisberg, S., 2019. An {R} Companion to Applied Regression, Third ed. Sage, Thousand Oaks CA https://socialsciences.mcmaster.ca/jfox/Books/Companion/>.
Frair, J.L., Merrill, E.H., Visscher, D.R., Fortin, D., Beyer, H.L., Morales, J.M., 2005. Scales of movement by elk *(Cervus elaphus)* in response to heterogeneity in forage resources and predation risk. Landsc. Ecol. 20 (3), 273–287.
Gillespie, T.W., Foody, G.M., Rocchini, D., Giorgi, A.P., Saatchi, S., 2008. Measuring and modelling biodiversity from space. Prog. Phys. Geogr. 32 (2), 203–221.

Gorelick, N., Hancher, M., Dixon, M., Ilyushchenko, S., Thau, D., Moore, R., 2017. Google earth engine: planetary-scale geo-spatial analysis for everyone. Remote Sens. Environ. 202, 18–27.
Guo, X., Wilmhurst, J., McCanny, S., Fargey, P., Richard, P., 2004. Measuring spatial and vertical heterogeneity of grasslands using remote sensing techniques. J. Environ. Inf. 3 (1), 24–32.
Guthery, F.S., Brennan, L.A., Peterson, M.J., Lusk, J.J., 2005. Information theory in wildlife science: critique and viewpoint. J. Wildl. Manag. 69 (2), 457–465.
Hall-Beyer, M., 2017. GLCM Texture: A Tutorial v. 3.0 March 2017. University of Calgary, Alberta, Canada.
Hanni, D.J., White, C.M., Van Lanen, N.J., Birek, J.J., Berven, J.M., McLaren, M.F., 2016. Integrated Monitoring in Bird Conservation Regions (IMBCR): Field Protocol for Spatially-Balanced Sampling of Landbird Populations. Unpublished report. Bird Conservancy of the Rockies, Brighton, Colorado, USA.
Hansen, M.C., Potapov, P.V., Moore, R., Hancher, M., Turubanova, S.A., Tyukavina, A., Thau, D., Stehman, S.V., Goetz, S.J., Loveland, T.R., Kommareddy, A., Egorov, A., Chini, L., Justice, C.O., Townshend, J.R.G., 2013. High-resolution global maps of 21st-century forest cover change. Science 342 (6160), 850–853.
Haralick, R.M., Shanmugam, K., Dinstein, I., 1973. Textural features for image classification. IEEE Trans. Syst. Man Cybernet. 3 (6), 610–621.
Homer, C.G., Dewitz, J.A., Jin, S., Xian, G., Costello, C., Danielson, P., Gass, L., Funk, M., Wickham, J., Stehman, S., Auch, R.F., Riitters, K.H., 2020. Conterminous United States land cover change patterns 2001–2016 from the 2016 National Land Cover Database. ISPRS J. Photogramm. Remote Sens. 162, 184–199.
Huete, A., Didan, K., Miura, T., Rodriguez, E.P., Gao, X., Ferreira, L.G., 2002. Overview of the radiometric and biophysical performance of the MODIS vegetation indices. Remote Sens. Environ. 83 (1–2), 195–213.
IUCN [International Union for Conservation of Nature and Natural Resources], 2020. The IUCN Red List of Threatened Species. Version 2020–1. https://www.iucnredlist.org.
Jacobs, R.B., Thompson, F.R., Koford, R.R., La Sorte, F.A., Woodward, H.D., Fitzgerald, J. A., 2012. Habitat and landscape effects on abundance of Missouri's grassland birds. J. Wildl. Manag. 76 (2), 372–381.
Jakubauskas, M.F., 1997. Effects of forest succession on texture in Landsat thematic mapper imagery. Can. J. Remote. Sens. 23 (3), 257–263.
Jetz, W., McGeoch, M.A., Guralnick, R., Ferrier, S., Beck, J., Costello, M.J., Fernandez, M., Geller, G.N., Keil, P., Merow, C., Meyer, C., Muller-Karger, F.E., Pereira, H.M., Regan, E.C., Schmeller, D.S., Turak, E., 2019. Essential biodiversity variables for mapping and monitoring species populations. Nat. Ecol. Evol. 3 (4), 539–551.
Jirinec, V., Isdell, R.E., Leu, M., 2016. Prey availability and habitat structure explain breeding space use of a migratory songbird. Condor 118 (2), 309–328.
Kayitakire, F., Hamel, C., Defourny, P., 2006. Retrieving forest structure variables based on image texture analysis and IKONOS-2 imagery. Remote Sens. Enviorn. 102, 390–401.
Lee, P.Y., Rotenberry, J.T., 2005. Relationships between bird species and tree species assemblages in forested habitats of eastern North America. J. Biogeogr. 32 (7), 1139–1150.
Loarie, S.R., Tambling, C.J., Asner, G.P., 2013. Lion hunting behavior and vegetation structure in an African savanna. Anim. Behav. 85 (5), 899–906.
Lopatin, J., Galleguillos, M., Fassnacht, F.E., Ceballos, A., Hernandez, J., 2015. Using a multispectral object-based lidar approach to estimate vascular plant richness in Mediterranean forests with complex structure. IEEE Geosci. Remote Sens. Lett. 12 (5), 1008–1012.
Lussem, U., Bolten, A., Menne, J., Gnyp, M.L., Schellberg, J., Bareth, G., 2019. Estimating biomass in temperate grassland with high resolution canopy surface models from UAV-based RGB images and vegetation indices. J. Appl. Remote. Sens. 13 (3), 1–26.
Mac Nally, R., 2000. Regression and model-building in conservation biology, biogeography and ecology: the distinction between – and reconciliation of – 'predictive' and 'explanatory' models. Biodivers. Conserv. 9 (5), 655–671.
MacArthur, R., MacArthur, J.W., 1961. On bird species diversity. Ecology 42, 594–598.
McCoy, E.D., Bell, S.S., 1991. Habitat structure: The evolution and diversification of a complex topic. In: Jones, B.S., Smith, R.Z. (Eds.), Habitat Structure: The Physical Arrangement of Objects in Space. Chapman and Hall, London, pp. 3–27.
Melin, M., Matala, J., Mehtatalo, L., Tiilikainen, R., Tikkanen, O.P., Maltamo, M., Pusenius, J., Packalen, P., 2014. Moose *(Alces alces)* reacts to high summer temperatures by utilizing thermal shelters in boreal forests- an analysis based on airborne laser scanning of the canopy structure at moose locations. Glob. Chang. Biol. 20 (4), 1115–1125.
Morley, P.J., Donoghue, D.N.M., Chen, J.C., Jump, A.S., 2019. Quantifying structural diversity to better estimate change at mountain forest margins. Remote Sens. Environ. 223, 291–306.
Nagendra, H., Rocchini, D., 2008. High resolution satellite imagery for tropical biodiversity studies: the devil is in the detail. Biodivers. Conserv. 17 (14), 3431–3442.
NEON (National Ecological Observatory Network), 2020. Data products NEON. DP3.30015.001, NEON.DP1.10098.001, NEON.DP1.10058.001, NEON. DP1.10003.001. Batelle, Boulder, CO, USA. http://data.neonscience.org (Accessed date: 23 January 2020).
Noss, R.F., 1990. Indicators for monitoring biodiversity: a hierarchical approach. Conserv. Biol. 4 (4), 355–364.
O'Brien, S.T., Hubbell, S.P., Spiro, P., Condit, R., Foster, R.B., 1995. Diameter, height, crown, and age relationships in eight neotropical tree species. Ecology 76 (6), 1926–1939.
Ozdemir, I., Karnieli, A., 2011. Predicting forest structural parameters using the image texture derived from WorldView-2 multispectral imagery in a dryland forest, Israel. Int. J. Appl. Earth Obs. Geoinf. 13 (5), 701–710.
Ozdemir, I., Mert, A., Ozkan, U.Y., Aksan, S., Unal, Y., 2018. Predicting bird species richness and micro-habitat diversity using satellite data. For. Ecol. Manag. 424, 483–493.
Patthey, P., Signorell, N., Rotelli, L., Arlettaz, R., 2012. Vegetation structural and compositional heterogeneity as a key feature in alpine black grouse microhabitat selection: conservation management implications. Eur. J. Wildl. Res. 58, 59–70.
Pettorelli, N., Wegmann, M., Skidmore, A., Mucher, S., Dawson, T.P., Fernandez, M., Lucas, R., Schaepman, M.E., Wang, T., O'Connor, B., Jongman, R.H.G., Kempeneers, P., Sonnenschein, R., Leidner, A.K., Bohm, M., He, K.S., Nagendra, H., Dubois, G., Fatoyinbo, T., Hansen, M.C., Paganini, M., de Klerk, H.M., Asner, G.P., Kerr, J.T., Estes, A.B., Schmeller, D.S., Heiden, U., Rocchini, D., Pereira, H.M., Turak, E., Fernandez, N., Lausch, A., Cho, M.A., Alcaraz-Segura, D., McGeoch, M.A., Turner, W., Mueller, A., St-Louis, V., Penner, J., Vihervaara, P., Belward, A., Reyers, B., Geller, G.N., 2016. Framing the concept of satellite remote sensing essential biodiversity variables: challenges and future directions. Remote Sens. Ecol. Conserv. 3 (2), 53–56.
R Core Team, 2020. R: A Language and Environment for Statistical Computing. Vienna, Austria. http://www.R-project.org/>.
Ralph, C.J., Geupel, G.R., Pyle, P., Martin, T.E., DeSante, D.F., 1993. Handbook of field methods for monitoring landbirds. Gen. Tech. Rep. PSW-GTR-144-www. Pacific Southwest Research Station, Forest Service, U.S. Department of Agriculture, Albany, CA (41 p).
Rhodes, C.J., Henrys, P., Siriwardena, G.M., Whittingham, M.J., Norton, L.R., 2015. The relative value of field survey and remote sensing for biodiversity assessment. Methods Ecol. Evol. 6, 772–781.
Rocchini, D., 2007. Effects of spatial and spectral resolution in estimating ecosystem alpha-diversity by satellite imagery. Remote Sens. Environ. 111 (4), 423–434.
Rocchini, D., Balkenhol, N., Carter, G.A., Foody, G.M., Gillespie, T.W., He, K.S., Kark, S., Levin, N., Lucas, K., Luoto, M., Nagendra, H., Oldeland, J., Ricotta, C., Southworth, J., Neteler, M., 2010. Remotely sensed spectral heterogeneity as a proxy of species diversity: recent advances and open challenges. Ecol. Inform. 5 (5), 318–329.
Rocchini, D., Boyd, D.S., Feret, J.-B., Foody, G.M., He, K.S., Lausch, A., Nagendra, H., Wegmann, M., Pettorelli, N., 2016. Satellite remote sensing to monitor species diversity: potential and pitfalls. Remote Sens. Ecol. Conserv. 2 (1), 25–36.
Rotenberry, J.T., 1985. The role of habitat in avian community composition: Physiognomy or floristics? Oecologia 67 (2), 213–217. https://doi.org/10.1007/BF00384286.
Schuldt, A., Ebeling, A., Kunz, M., Staab, M., Guimaraes-Steinicke, C., Bachmann, D., Buchmann, N., Durka, W., Fichtner, A., Fornoff, F., Hardtle, W., Hertzog, L.R., Klein, A.-M., Roscher, C., Schaller, J., von Oheimg, G., Weigelt, A., Weisser, W., Wirth, C., Zhang, J., Bruelheide, H., Eisenhauer, N., 2019. Multiple plant diversity components drive consumer communities across ecosystems. Nat. Commun. 10, 1–11.
Seibold, S., Hempel, A., Piehl, S., Bassler, C., Brandl, R., Rosner, S., Muller, J., 2013. Forest vegetation structure has more influence on predation risk of artificial ground nests than human activities. Basic Appl. Ecol. 14 (8), 687–693.
Sheeren, D., Bonthoux, S., Balent, G., 2014. Modeling bird communities using unclassified remote sensing imagery: effects of the spatial resolution and data period. Ecol. Indic. 43, 69–82.
Simonson, W.D., Allen, H.D., Coomes, D.A., 2014. Applications of airborne lidar for the assessment of animal species diversity. Methods Ecol. Evol. 5 (8), 719–729.
Skowno, A.L., Bond, W.J., 2003. Bird community composition in an actively managed savanna reserve, importance of vegetation structure and vegetation composition. Biodivers. Conserv. 12 (11), 2279–2294.
Stein, A., Gerstner, K., Kreft, H., 2014. Environmental heterogeneity as a universal driver of species richness across taxa, biomes and spatial scales. Ecol. Lett. 17 (7), 866–880.
St-Louis, V., Pidgeon, A.M., Radeloff, V.C., Hawbaker, T.J., Clayton, M.K., 2006. High-resolution image texture as a predictor of bird species richness. Remote Sens. Environ. 105 (4), 299–312.
St-Louis, V., Pidgeon, A.M., Clayton, M.K., Locke, B.A., Bash, D., Radeloff, V.C., 2009. Satellite image texture and a vegetation index predict avian biodiversity in the Chihuahuan Desert of New Mexico. Ecography 32 (3), 468–480.
Tews, J., Brose, U., Grimm, V., Tielborger, K., Wichmann, M.C., Schwager, M., Jeltsch, F., 2004. Animal species diversity driven by habitat heterogeneity/diversity: the importance of keystone structures. J. Biogeogr. 31 (1), 79–92.
Thorpe, A.S., Barnett, D.T., Elmendorf, S.C., Hinckley, E.L.S., Hoekman, D., Jones, K.D., LeVan, K.E., Meier, C.L., Stanish, L.F., Thibault, K.M., 2016. Introduction to the sampling designs of the National Ecological Observatory Network Terrestrial Observation System. Ecosphere 7 (12), 1–11.
Tuanmu, M.-N., Jetz, W., 2015. A global, remote sensing-based characterization of terrestrial habitat heterogeneity for biodiversity and ecosystem modelling. Glob. Ecol. Biogeogr. 24 (11), 1329–1339.
Virah-Sawmy, M., Gillson, L., Willis, K.J., 2009. How does spatial heterogeneity influence resilience to climatic changes? Ecol. Monogr. 79 (4), 557–574.
Vogeler, J.C., Hudak, A.T., Vierling, L.A., Evans, J., Green, P., Vierling, K.T., 2014. Terrain and vegetation structural influences on local avian species richness in two mixed-conifer forests. Remote Sens. Environ. 147, 13–22.
Wallis, C.I.B., Paulsch, D., Zeilinger, J., Silva, B., Fernandez, G.F.C., Brandl, R., Farwig, N., Bendix, J., 2016. Contrasting performance of Lidar and optical texture models in predicting avian diversity in a tropical mountain forest. Remote Sens. Environ. 174, 223–232.
Walsh, C., Mac Nally, R., 2013. hier.Part: Hierarchical Partitioning. R Package Version 1.0-4. https://CRAN.R-project.org/package=hier.part>.
Wang, R., Gamon, J.A., 2019. Remote sensing of terrestrial plant biodiversity. Remote Sens. Environ. 231, 1–15.

Wood, E.M., Pidgeon, A.M., Radeloff, V.C., Keuler, N.S., 2012. Image texture as a remotely sensed measure of vegetation structure. Remote Sens. Environ. 121, 516–526.
Wood, E.M., Pidgeon, A.M., Radeloff, V.C., Keuler, N.S., 2013. Image texture predicts avian density and species richness. PLoS One 8 (5), 1–14.
Zhao, S., Fang, J., Peng, C., Tang, Z., 2006. Relationships between species richness of vascular plants and terrestrial vertebrates in China: analyses based on data of nature reserves. Bio. Res. 12 (2), 189–194.